

Influence of oxygen ion implantation on the free volume parameters and electrical conductivity of a polymer-based bakelite RPC detector material

K. V. Aneesh Kumar,¹ G. N. Kumaraswamy,² C. Ranganathaiah,³ H. B. Ravikumar¹

¹Department of Studies in Physics, University of Mysore, Manasagangothri, Mysuru 570006, India

²Department of Physics, Amrita School of Engineering, Amrita Vishwa Vidyapeetham, Bengaluru 560035, India

³JSS Technical Institutions, JSSTI Campus, Mysuru 570006, India

Correspondence to: H. B. Ravikumar (E-mail: hbr@physics.uni-mysore.ac.in)

ABSTRACT: We have investigated the effect of ion implantation on structural modification and the electrical conductivity of Bakelite-resistive plate chamber (RPC) detector material used in high energy physics experiments. Samples of Bakelite polymer were exposed to 100 keV and 150 keV oxygen ions in the fluence of 10^{12} to 10^{15} ions cm^{-2} . Ion implantation induced microstructural changes have been studied using positron annihilation lifetime spectroscopy, X-ray diffraction and Fourier transform infrared techniques. Positron lifetime parameters viz., *o*-Ps lifetime and its intensity showed formation of radicals, secondary ions due to the creation of interior tracks by high-energy ions followed by chain scission at lower fluence of 100 keV implantation. The decreased free volume size at 150 keV ion implantation is an indication of crosslinking and filling up of interior tracks by the implanted ions. Variation of ac conductivity with frequency obeys Jonscher power law at 100 keV and the conduction mechanism is explained by barrier hopping model. © 2017 Wiley Periodicals, Inc. *J. Appl. Polym. Sci.* **2017**, *134*, 44962.

KEYWORDS: ageing; crosslinking; free volume; morphology

Received 12 June 2016; accepted 31 January 2017

DOI: 10.1002/app.44962

INTRODUCTION

India-based Neutrino Observatory (INO) is a multi-institutional collaborative project to construct a world-class underground laboratory for high energy physics, astrophysics, and nuclear physics experiments in India.¹ The primary goal of this basic science project is to study the neutrinos and its mysterious properties from various natural and laboratory sources. The resistive plate chambers (RPCs)² are widely used as the active detectors in this high-energy physics experiment. These RPCs are made up of high-resistive materials like glass or Bakelite polymer. The RPC detectors are extensively used in radiation rich environments and they are constantly exposed to high energetic charged particles like cosmic ray muons, protons, electrons, etc. It is also true that RPC detectors are operated at high operating voltages for longer duration, which will affect their time resolution and efficiency.³ Bakelite RPCs exhibit undesirable high leakage current compared to glass RPCs due to polymer aging.^{4,5} Therefore, it is important to understand the microstructural properties to find the origin of large leakage

current exhibited by the Bakelite polymer RPC detector material.

It is well documented that the irradiation of high energetic radiations like gamma rays, electrons, and the implantation of ions play a significant role in the structural modification of the polymers.^{6,7} The structural alterations in the ion-implanted polymers are resulted due to drastic changes in the chemical and physical properties of the polymer network. The changes in the microstructural and physical properties of the ion-implanted polymers are mainly due to the crosslinking, chain scission, chain aggregation, double bond formation and molecular emission by radical reactions.^{8–12} These processes depend on the structure of polymer matrix, ion implantation energy, and the energy transfer mechanism.⁸ In addition, the effect of stopping of incoming ions accompanied by the creation of high-energy interior tracks in the polymer matrix cannot be ruled out.

Based on our previous studies on electron beam irradiation induced structural changes,¹¹ it has been found that it is more significant to conduct experimental investigations on the ion

Additional Supporting Information may be found in the online version of this article.

© 2017 Wiley Periodicals, Inc.

implantation induced microstructural changes of Bakelite RPC detector material. We expect that the implantation of lighter ions such as oxygen and argon with low energy may modify the microstructure of Bakelite without damaging the actual properties of the material. Moreover, the detailed literature survey reveals that such type of studies on Bakelite RPC detector material have no where reported. Therefore, in the present study, we have carried out microstructural characterization of 100 keV and 150 keV O^+ ions implanted Bakelite RPC detector material with different implantation fluences. The microstructural characterization has been performed by making use of one of the well sophisticated technique viz., Positron Annihilation Lifetime Spectroscopy (PALS).¹³

In polymers, *ortho*-positronium (*o*-Ps) lifetime is an important parameter of positron annihilation lifetime studies as *o*-Ps trapped and annihilated in free volume sites and therefore determines the size of free volume holes in the polymer matrix,^{11,14} which has direct bearing on the microstructure. These free volume holes provide pathways for thermal motion of the chain segments. The relaxation processes in polymers are well described by considering the free volume as an internal material parameter. In this study, an attempt has been made to correlate the free volume properties with conductivity of O^+ ions implanted Bakelite RPC detector material. Other experimental techniques such as XRD, FTIR, and SEM are used to explore the effects of ion implantation on Bakelite RPC detector material and complimentary to PALS. The simulation program viz., stopping and range of ions in matter (SRIM) and transport of ions in matter (TRIM) are also used to ensure the interaction of O^+ ions and depth of trapping in Bakelite polymer material.

Recently, Pradhan *et al.*¹⁵ and Hadjichristov *et al.*¹⁶ have reported the ac conduction mechanism and its interesting properties on different polymers. Motivated by these studies, we have also carried out ac conductivity studies and evaluated the frequency exponent “*S*” values on different energy and fluences at room temperature. The behavior of “*S*” value with increase of ion implantation energy and fluences can be explained according to correlated barrier hopping model (CBH). In CBH model, the charge carrier’s hop between the sites over the potential barrier determines the electrical conductivity, which depends on the free volume hole size. These investigations will throw light on the problem of large leakage current observed in Bakelite RPC detector material. Furthermore, this will also provide the necessary information on O^+ ion implantation induced effects upon various energies and fluences for the RPC detector fabrication. We expect the improvement in the performance of Bakelite polymer with the implantation of O^+ ions of appropriate energy and fluences.

EXPERIMENTAL

Oxygen Ion Implantation

Bakelite samples (P-120, Matt finished NIMA LI-1989, Grade XXX) of density 1.22 g cm^{-3} manufactured by Bakelite Hylam, India were collected from Variable Energy Cyclotron Centre, Kolkata in the form of sheets. The same Bakelite samples are used for the fabrication of RPC detectors in INO research project. The chemical structure of Bakelite is shown in

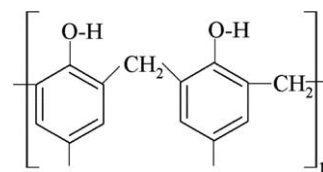


Figure 1. The chemical structure of Bakelite.

Figure 1. The rectangular samples having dimensions of $1 \text{ cm} \times 1 \text{ cm}$ and thickness 0.20 cm were implanted with 100 keV and 150 keV O^+ ion (+1 charge and $1 \mu\text{A}$ current) from Inter-University Accelerator Center (IUAC), New Delhi, India at different fluences 1×10^{12} , 1×10^{13} , 1×10^{14} , and 1×10^{15} ions cm^{-2} . These samples were used for PALS, XRD, SEM, FTIR, AC, and DC electrical conductivity measurements.

X-ray Diffraction Studies

XRD spectra of as received and O^+ ion-implanted Bakelite samples at different energies and fluences have been recorded using powder X-ray diffractometer RIGAKU-DENKI II miniflex with Ni filtered $\text{Cu-K}\alpha$ X-rays of wavelength 1.5406 \AA . The X-ray scanning was performed in the 2θ range 6 to 60° with scanning steps of 0.001° . Crystallinity was calculated from the ratio of area under the crystalline peaks to the total area using computer program Peakfit 4.1.

Positron Annihilation Lifetime Measurements

Positron annihilation lifetime spectra were recorded for as received and O^+ ion-implanted Bakelite samples using positron lifetime spectrometer. The positron lifetime spectrometer consists of a fast-fast coincidence system with BaF_2 scintillators coupled with photomultiplier tubes type XP2020/Q with quartz window as detectors. BaF_2 scintillators are conical to achieve better time resolution. Two identical pieces of the samples were placed on either sides of $15 \mu\text{Ci-}^{22}\text{Na}$ positron source deposited on a pure Kapton foil of thickness 0.0127 mm . This sample-source sandwich was placed between the two detectors of positron lifetime spectrometer operated at 230 ps time resolution to acquire lifetime spectrum. Two to three positron lifetime spectra with more than a million counts under each spectrum were recorded in a time of 2 to 4 h. Consistently reproducible spectra were analyzed into three lifetime components with the help of a computer program PATFIT-88¹⁷ with proper source and background corrections. Source correction term and resolution function were estimated from the lifetime of well-annealed aluminum using RESOLUTION program.¹⁷ Three Gaussian resolution functions were used in the analysis of positron lifetime spectra of Bakelite samples.

The *o*-Ps lifetime (τ_3) is related to the free volume hole size by a simple relation given by Nakanishi *et al.*,¹⁸ which was developed on the basis of theoretical models originally proposed by Tao for molecular liquids and later by Eldrup *et al.*¹⁹ In this model, Positronium is assumed to be localized in a spherical potential well having an infinite potential barrier of radius R_0 with an electron layer in the region $R < r < R_0$. The relation between “ τ_3 ” and the radius R of the free volume hole or cavity is,

$$\lambda = \frac{1}{\tau_3} = 2P = 2 \left[1 - \left(\frac{R}{R_0} \right) + \left(\frac{1}{2\pi} \right) \sin \left(\frac{2\pi R}{R_0} \right) \right] \text{ns}^{-1} \quad (1)$$

where $R_0 = R + \delta R$ and δR is an adjustable parameter.

By fitting eq. (1) with τ_3 values for known hole sizes in porous materials like zeolites, a value of $\delta R = 0.1657$ nm was obtained. With this value of δR , the free volume radius R has been calculated from eq. (1) and the average size of free volume holes (V_f) is evaluated as

$$V_f = (4/3) \pi R^3 \quad (2)$$

The fractional free volume or the free volume content (F_v), can also be estimated as

$$F_v = C V_f I_3 \quad (3)$$

where C is structural constant, 0.0018 \AA^3 , V_f is the free volume hole size, and I_3 is the *o*-Ps intensity.

FTIR Characterization and Scanning Electron Microscopy (SEM) Studies

FTIR Spectra for as-received and ion-implanted Bakelite samples at the two energy levels upon different fluences were recorded in the wave number range of 4000 to 600 cm^{-1} using Spectrum Two 94012 Spectrometer with a resolution of 4 cm^{-1} . Surface morphology of as received and ion-implanted samples were also studied using Scanning Electron Microscope (SEM) Zeiss-EVO LSI5 Model.

Electrical Conductivity Measurements

The electrical conductivity of as received and ion-implanted Bakelite samples at different fluences were evaluated at room temperature. The dc electrical conductivity of Bakelite samples of dimension $1 \text{ cm} \times 1 \text{ cm} \times 0.20 \text{ cm}$ was measured using Keithley 2636A system Source Meter. The sample was sandwiched between two electrodes pasted with silver paste. Lab Tracer 2.0 Source Meter-Integration software was used to record the voltage and current data. From the recorded voltage and current data, the value of bulk resistance (R_b) was calculated. The dc electrical conductivity (σ) was obtained for different fluences using the relation: $\sigma = \frac{t}{R_b A}$, where t and A are the thickness and area of contact of the sample under study respectively. Ac conductivity measurements were also made using LCR Hi Tester Hioki (Japan) 3532-50 programmable computer interfaced digital LCR impedance meter in the frequency range of 100 Hz to 5 MHz at room temperature. The measured conductance $G(\omega)$ was used to calculate ac conductivity of as received and ion-implanted Bakelite samples using the relation: $\sigma = \frac{G(\omega)t}{A}$, where $G(\omega)$ is the measured conductance.

RESULTS AND DISCUSSION

SEM Results

SEM micrograph of as received Bakelite polymer detector material sample exhibits remarkable surface morphological changes upon O^+ ion implantation. Figure 2(a,b) shows the SEM micrographs of 100 and 150 keV O^+ ion-implanted Bakelite samples respectively. They exhibit heterogeneous distribution of pores at the implantation fluence $10^{12} \text{ ions cm}^{-2}$ and show increased pore size at higher implantation fluences at 100 keV . The increased pore size especially at $10^{13} \text{ ions cm}^{-2}$ O^+ ion

implantation fluence indicates the structural damage due to the formation of energetic O^+ ion track and scission of polymeric chains.²⁰ The pore size reduces at 150 keV O^+ ion implantation due to the crosslinking of polymeric chains by the radicals and implanted O^+ ions.^{21,22} SEM micrographs reveal that the surface roughness of Bakelite samples vary with both O^+ ion implantation energy and fluences. This will alter the surface resistivity of RPC detector and hence its performance.²³⁻²⁵

Positron Annihilation Lifetime Spectroscopy Results

The microstructural changes of Bakelite polymer upon 100 keV and 150 keV O^+ ion implantation is clearly revealed by positron lifetime studies. As we are interested in free volume cavity size and their concentration in Bakelite samples, only the third and long lifetime component viz., *o*-Ps lifetime (τ_3) and *o*-Ps intensity (I_3) derived from PATFIT-88 program are reported here. Figure 3(a,b) represents the variation of *o*-Ps lifetime (τ_3), free volume size (V_f), and *o*-Ps intensity (I_3) at 100 keV and 150 keV O^+ ion-implanted Bakelite samples, respectively. It was verified from the SRIM analysis of 100 keV and 150 keV O^+ ion implantation that, along with the surface morphological changes ion implantation also alters the bulk properties of the Bakelite polymer. It was reported that the experimentally obtained depth distributions of the implanted ions in many polymers differ significantly from the simulated ones,⁸ which is well supported by our reported PALS results. Recently, Al-Qaradawi *et al.*²⁶ reported the formation of defects in the bulk of polyethylene by ion bombardment. The stopping of incoming high-energy ions in the polymer matrix are accompanied by creation of high-energy interior tracks and leads to the formation of radicals, secondary ions, and electrons.²⁷ The structural alterations of the implanted polymer layers result in the drastic changes in PALS parameters and hence the related properties.

From Figure 3(a), it is observed that *o*-Ps lifetime (τ_3) of Bakelite sample increases as a function of 100 keV O^+ ion implantation fluence and exhibit about 330 ps increase from as received to $10^{14} \text{ ions cm}^{-2}$ implantation fluence. After that, there is about 118 ps reduction in *o*-Ps lifetime at $10^{15} \text{ ions cm}^{-2}$ fluence. The free volume size also increases continuously and shows about 30 \AA^3 increase from as received to $10^{14} \text{ ions cm}^{-2}$ and then decreases to 83.92 \AA^3 at $10^{15} \text{ ions cm}^{-2}$ fluence. Similar types of results have been reported in the literature by Popok,⁸ Kavetsky *et al.*,⁹ and Shariff *et al.*²⁸ for various ion-implanted polymers. They attributed these variations in ion-implanted polymers to chain scission, crosslinking and creation of interior ion tracks. Based on the literature evidences, the variation of *o*-Ps lifetime and free volume hole sizes in the present study can be explained as below.

The positronium (Ps) formation takes place preferentially at the free volume cavities, which are the regions of low electron density exist mainly in the amorphous domains of polymers. The energetic implanted ions will create interior ion tracks by imparting some of its momentum into the bulk of Bakelite. This may result in the scission of weaker polymer chains, produces large number of mobile radicals at the polymer bulk and increases the free volume hole sizes.^{9,10,28} Therefore, 330 ps increase in *o*-Ps lifetime and 30 \AA^3 in free volume size from the

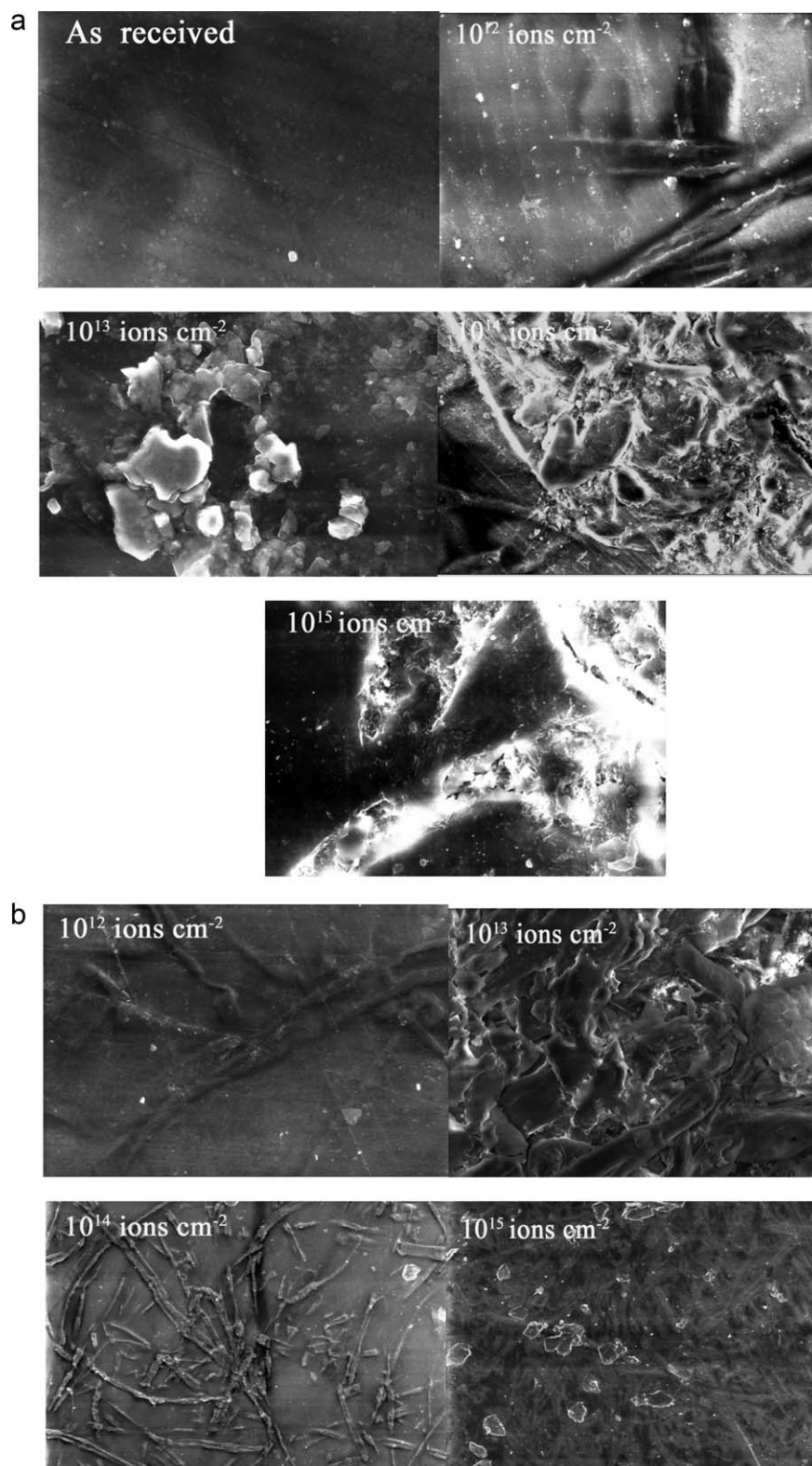


Figure 2. (a) SEM micrographs of as received and 100 keV O^+ ion-implanted Bakelite samples at different fluences (10^{12} – 10^{15} ions cm^{-2}). (b) SEM micrographs of 150 keV O^+ ion-implanted Bakelite samples at different fluences (10^{12} – 10^{15} ions cm^{-2}).

as received to O^+ ion implantation fluence at 10^{14} ions cm^{-2} is attributed to the chain scission. The remarkable decrease in *o*-Ps lifetime (118 ps) and free volume size (10.82 \AA^3) from 10^{14}

to 10^{15} ions cm^{-2} fluence may be due to the crosslinking of polymeric chains of Bakelite. The formation of crosslinks occurs by the induced radical reactions between the polymeric chains

of Bakelite. These reactions are carried by the radicals formed during the scission of polymeric chains in the initial stages of O^+ ion implantation.^{11,29}

From Figure 3(b), it is clearly observed that the *o*-Ps intensity (I_3) decreases from as received 13.27% to 7.55% at 10^{14} ions cm^{-2} fluence and show a marginal increase of about 1.8% from 7.55% to 9.34% at 10^{15} ions cm^{-2} fluence. The decrease in I_3 may be due to the inhibition of positronium (Ps) formation by the free radical formations. The cleavage of weaker bonds in Bakelite yield phenyl radicals and OH^- ions. These radicals undergo fast reactions with the electrons of the spur created during slowing down of positrons and may cause ionization or oxidation and thereby inhibits the formation of positronium.³⁰ The increase in *o*-Ps intensity from 10^{14} to 10^{15} ions cm^{-2} fluences is due to the structural modification of Bakelite induced by the chain scission followed by crosslinking of the polymer chains.

The variation of free volume size (V_f) at 150 keV O^+ ion implantation can also be explained on the same line. At 150 keV, the free volume size (V_f) decreases from 64.90 \AA^3 to 57.98 \AA^3 upon implantation of O^+ ions in the fluence 10^{14} ions cm^{-2} . However, there is a noticeable increase of about 170 ps in *o*-Ps lifetime (τ_3) and 14 \AA^3 free volume size (V_f) is observed at 10^{15} ions cm^{-2} . The decrease in free volume size upon O^+ ion implantation at 10^{14} ions cm^{-2} fluence is attributed to the crosslinking of polymer chains by the radicals formed during the lower ion implantation fluences and filling up of ion tracks by the O^+ ions. It is well known that the bond dissociation energy of OH, CH, and CH_2 bonds in polymers does not exceed 10 eV. Therefore, the slight increase in free volume size upon 150 keV O^+ ion implantation at 10^{15} ions cm^{-2} fluence is attributed to the scission of OH, CH_2 bonds and the formation of interior ion tracks in the polymer due to high energetic ionic collision. In the process of O^+ ion implantation, the energetic ions penetrate in to few microns depth in the material and loose their energy by the inelastic collision with molecules of the polymer. In this process, some of its energy gets transferred to the side chains of the Bakelite polymer. At higher energies, the momentum of the implanted ion can displace the polymer chains from its original site and results in the cleavage of chemical bonds and hence create additional free volume cavities. This may be the major cause for the changes in the bulk properties of Bakelite upon ion implantation. Therefore, taking the energy deposited by high-energy implanted O^+ ions into the consideration, the formation of highly disordered area along the ion trajectory is known as latent track^{8,31} cannot be ruled out. The multiple breakages of the chemical bonds within and around the ion path may be the reason for the observed PALS results. Therefore, the increased free volume size is attributed to the scission of O—H bonds into H^+ and O^{2-} free radicals. The increased *o*-Ps intensity (I_3) at 150 keV (14.31% at 10^{14} ions cm^{-2}) is probably due to the creation of more number of smaller free volumes upon implantation of higher O^+ ion fluences.³² The formation of latent tracks and the energy deposition along the track core results in hardening of the polymer, which is reflected in the decrease in I_3 at higher fluences.²⁷

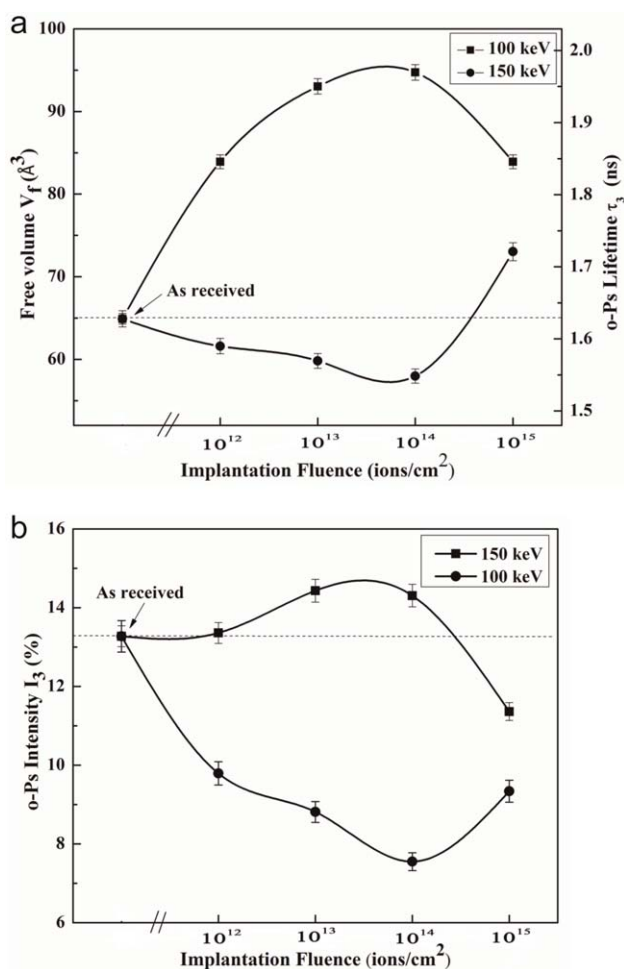


Figure 3. (a) The variation of *o*-Ps Lifetime (τ_3) and free volume (V_f) at 100 keV and 150 keV O^+ ion-implanted samples as a function of ion implantation fluences. (b) The variation of *o*-Ps Intensity (I_3) at 100 keV and 150 keV O^+ ion-implanted samples as a function of ion implantation fluences.

XRD Results

XRD spectra of as received and O^+ ion-implanted Bakelite samples at 100 and 150 keV energies are shown in Figure 4(a,b) respectively. Bakelite is highly amorphous in nature and exhibits about 19% of crystallinity. At 100 keV, the crystallinity of O^+ ion-implanted samples show a sharp decrease from 19% (as received) to 16.33% in the lower O^+ ion fluence (10^{13} ions cm^{-2}). After 10^{13} ions cm^{-2} , crystallinity of ion-implanted samples increases and shows maximum value at 10^{15} ions cm^{-2} fluence. The disappearance of the observed tiny peak at 2θ angles 31.6° and 39° of as received sample at higher fluences indicate the increased amorphosity of Bakelite upon O^+ ion implantation. This may be due to scission of polymeric chains of Bakelite.³³ The increased percentage of crystallinity at 10^{15} ions cm^{-2} fluence may be due to the crosslinking of polymeric chains of Bakelite owing to the radical reaction during ion implantation and hence close packing of the polymeric chains.⁸

The crystallinity of 150 keV O^+ ion-implanted samples show a sharp increase from 19% to 23% at 10^{12} ions cm^{-2}

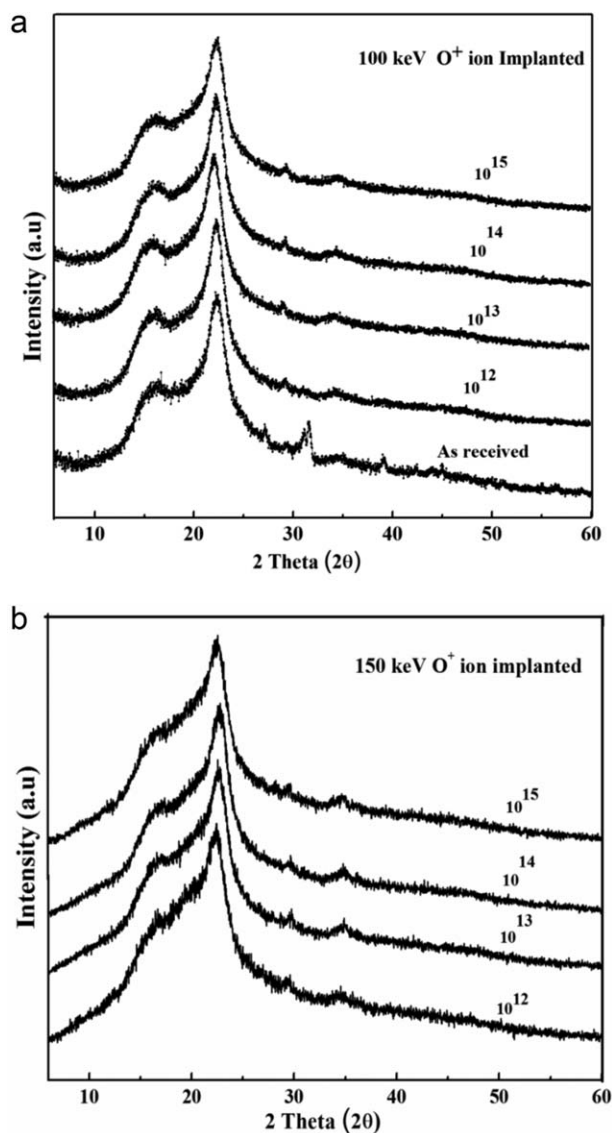


Figure 4. (a) XRD Spectra of as received and 100 keV ion-implanted Bakelite samples at different fluences (10^{12} – 10^{15} ions cm^{-2}). (b) XRD spectra of 150 keV ion-implanted Bakelite samples at different fluences (10^{12} – 10^{15} ions cm^{-2}).

implantation fluence. After that, the crystallinity of O^+ ion-implanted samples decreases slightly to 22% and then reduced to 18.54% at the implantation fluence 10^{15} ions cm^{-2} . The slight increase in crystallinity at the lower fluences indicates that the ion implantation improves the crystallinity of Bakelite material and hence the close packing. The increased percentage of crystallinity at the lower fluences may be due to the crosslinking of polymeric chains of Bakelite owing to the radical reaction during O^+ ion implantation. This is reflected in the reduced σ -Ps lifetime and free volume hole size of the reported PALS results. The variation of crystallinity and free volume as a function of ion implantation fluences at 100 and 150 keV are shown in Figure 5(a,b), respectively. The reported crystallinity and free volume hole size exhibit good correlation and corroborates well with the reported electrical conductivity results.

FTIR Results

The nature of chemical and structural modifications brought out by O^+ ion implantation at different energies and fluences can be understood by FTIR studies. The FTIR spectra of 100 and 150 keV Oxygen ion-implanted Bakelite sample with different O^+ ion implantation fluences are shown in Figure 6(a,b), respectively. As can be seen from the FTIR spectra [Figure 6(a)], the major transmittance bands in Bakelite polymer are at 3330 (Phenol/OH), 3016 (in phase stretching vibration of CH-alkane), 1739 (C–C aromatic ring/CH of CH_2), 1449 (CH-aliphatic/CH-deformation vibration), 1366 (CH-deformation), 1002 (C–O stretching vibrations of CH_2 –OH), and 809 cm^{-1} (CH-deformations) respectively.³⁴ From Figure 6(a,b), it is clear that there is no much change in the functional group corresponding to the wave numbers 1739, 1449, 1366, 1217 cm^{-1} upon ion implantation at both the energies. The functional groups viz., C–H aliphatic bridge, C–C aromatic ring and out of phase stretching vibration of $-\text{CH}_2-$ alkane may not undergo much chemical changes and the contribution of these functional groups for the structural modification of Bakelite are insignificant. However, the remarkable changes is observed in the wave number 3330 cm^{-1}

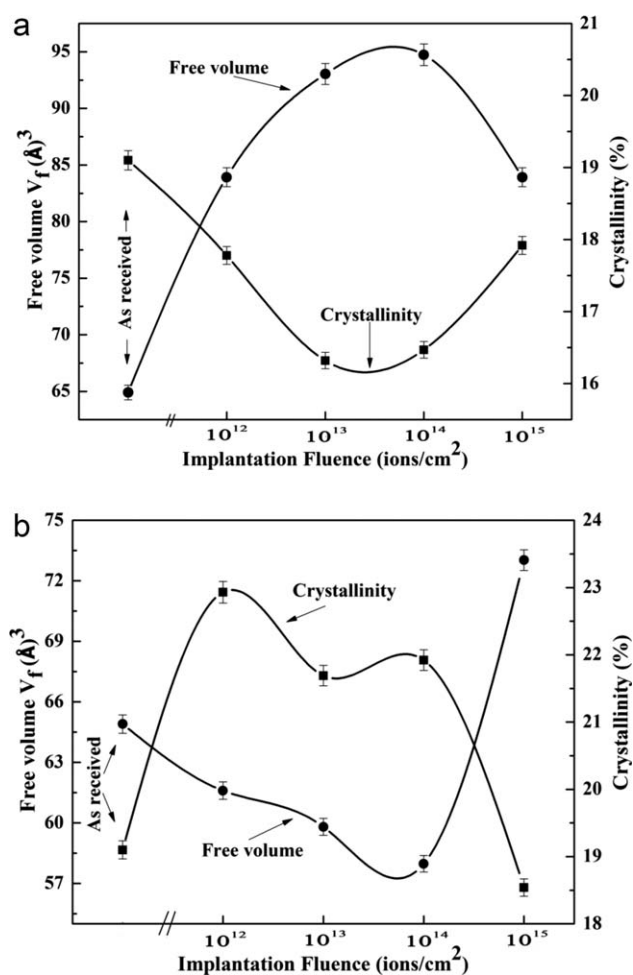


Figure 5. (a) The variation of free volume (V_f) and crystallinity as a function of ion implantation fluences at 100 keV. (b) The variation of free volume (V_f) and crystallinity as a function of ion implantation fluences at 150 keV.

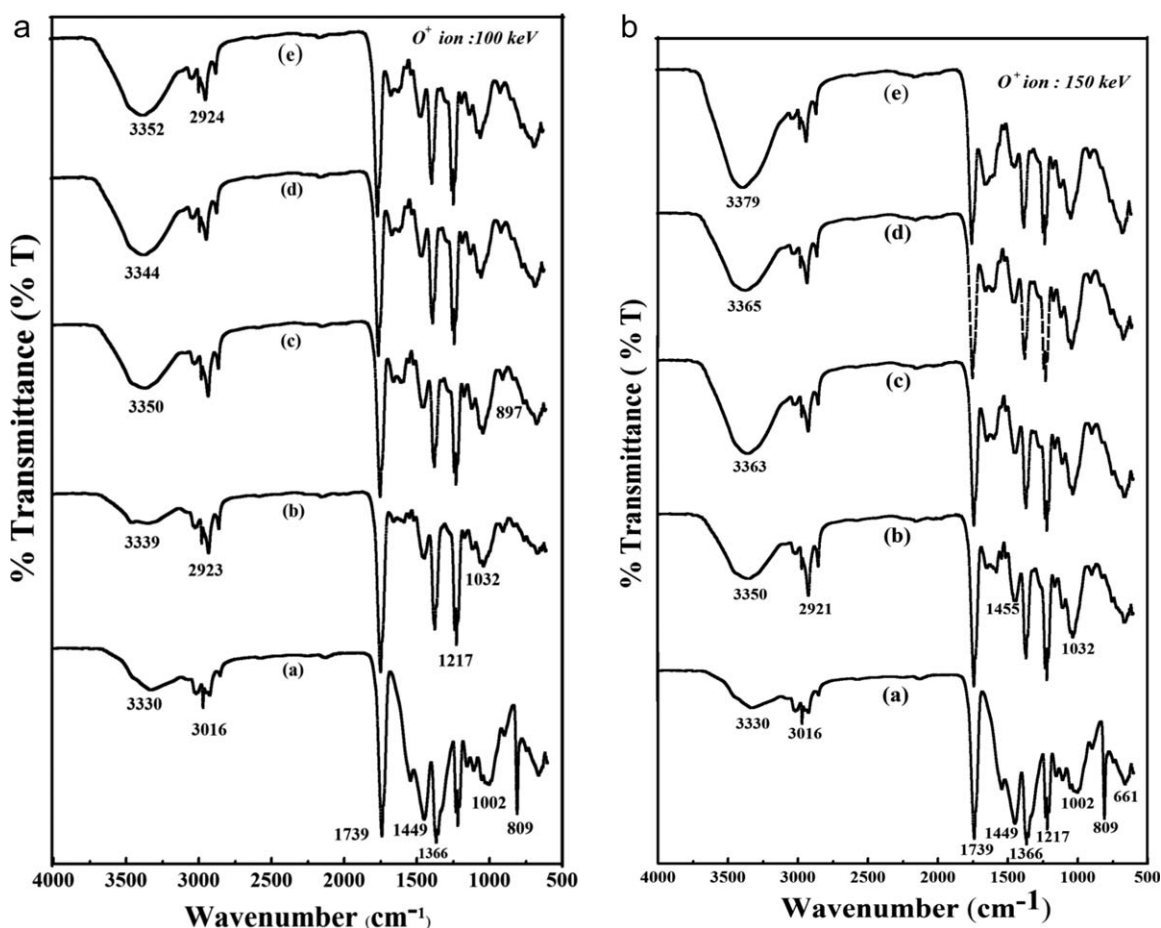


Figure 6. (a) FTIR Spectra of as received and 100 keV-ion-implanted Bakelite samples at different fluences [(a–e) represents as received, 10^{12} , 10^{13} , 10^{14} , and 10^{15} ions cm^{-2} fluences, respectively]. (b) FTIR Spectra of as received and 150 keV of ion-implanted Bakelite samples at different fluences [(a–e) represents as received, 10^{12} , 10^{13} , 10^{14} , and 10^{15} ions cm^{-2} fluences, respectively].

(Phenol/OH), 3016 cm^{-1} (in phase stretching vibration of CH-alkane), and 1002 cm^{-1} (single bond stretching vibrations of $-\text{CH}_2\text{OH}$) at 100 keV implantation energy. The transmittance band corresponding to Phenol/OH at 3330 cm^{-1} in the as received Bakelite shifted to 3350 cm^{-1} at 10^{13} ions cm^{-2} and remains at 3352 cm^{-1} for higher implantation fluences. The bands at 3330 cm^{-1} , 3016 cm^{-1} are shifted towards higher wave number and the percentage of transmittance decreases at lower fluences. This indicates the weakening of OH bonds and the stretching vibrations of CH alkane, which leads to the scission of Bakelite polymer chains.^{8,35}

A clear peak shift is observed in the wave number range of 3330 cm^{-1} upon 150 keV O⁺ ion implantation. The transmittance peak shifted continuously from 3330 cm^{-1} to 3379 cm^{-1} from as received to the implantation fluence 10^{15} ions cm^{-2} . The marginal shift in wave number and decreased percentage of transmittance (88% to 79%) confirms the variations of OH functional group and crosslinking upon ion implantation. This is complimentary with the reduced free volume hole size observed in PALS results. Again a clear change at the wave number 1002 cm^{-1} indicates the bending of C-O-H contributes to the polymer chain relaxation and thereby increases the free volume size. The remarkable changes in the peak at 809 cm^{-1}

at both the energies can be attributed to significant variation in the CH deformation upon O⁺ ion implantation. This also responsible for the chain relaxation and hence the free volume hole size. FTIR results confirm that ion implantation at lower energies will not affect the basic functional groups of Bakelite polymer chains and aromatic ring structure or chemical/physical properties much. However, it will cause significant changes only to phenolic/OH functional groups and stretching vibrations of CH groups, which will produces the free radicals or ions.³⁶ Hence, the chemical changes due to the rearrangement of free radicals after the chain cleavage and crosslinking upon ion implantation contributing much for the microstructural modifications. This is also reflected in the electrical conductivity results explained below.

DC Conductivity Results

Polymers are usually considered as good electrical insulators and a variety of their applications depends on this insulating property. Apart from the surface morphological information, the conductivity studies help us to better understand the method of charge transport in the Bakelite polymer. Therefore, based on the microstructural characterization of this material, one can find better correlation between free volume and electrical conductivity in Bakelite polymer material.

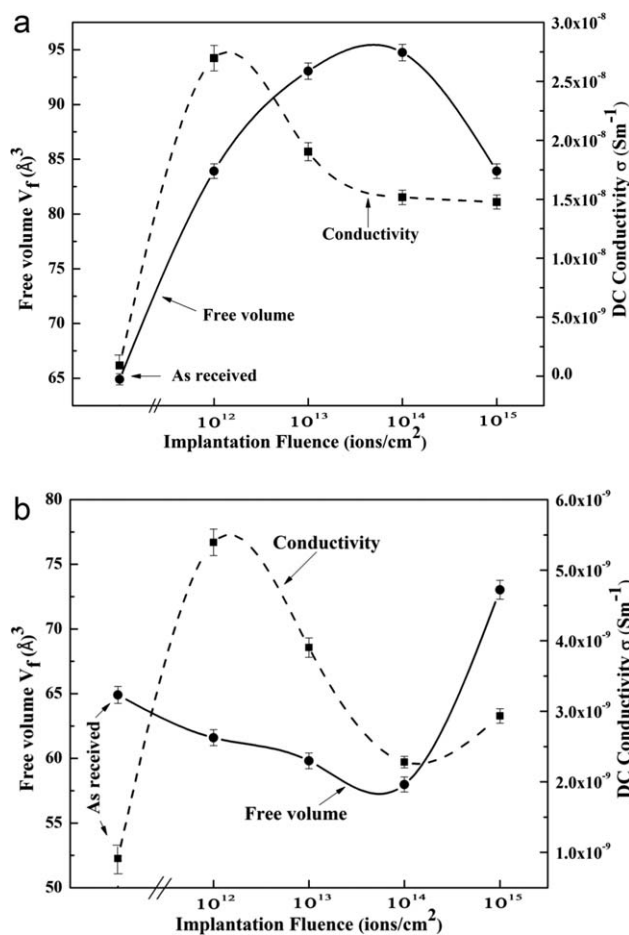


Figure 7. (a) The free volume and dc conductivity of as received and 100 keV ion-implanted Bakelite samples at different fluences. (b) The free volume and dc conductivity of as received and 150 keV ion-implanted Bakelite samples at different fluences.

Figure 7(a,b) shows the variation of both free volume and dc electrical conductivity of 100 and 150 keV O⁺ ion-implanted Bakelite sample as a function implantation fluences respectively. The dc conductivity of 100 keV ion-implanted samples increases and show about $2.69 \times 10^{-8} \text{ Sm}^{-1}$ at $10^{12} \text{ ions cm}^{-2}$, free volume size also shows similar trend. The increased electrical conductivity at the lower fluence is attributed to the scission of hydrogen bonded phenolic groups leading to the formation of OH⁻, H⁺ radicals.^{9,33} Even though, there is a slight increase in free volume hole size at the ion fluences 10^{13} and $10^{14} \text{ ions cm}^{-2}$, conductivity reduces marginally and shows $1.52 \times 10^{-8} \text{ Sm}^{-1}$ at the $10^{14} \text{ ions cm}^{-2}$ ion fluence. This reduction is probably due to the hindrance to mobility of ions owing to the initialization of crosslinking of the polymer chains. As the crosslinking is predominant after O⁺ ion fluence is $10^{14} \text{ ions cm}^{-2}$, the reduced void space restrict the movement of O⁺ ions and hence the electrical conductivity.^{37,38}

The dc conductivity of 150 keV O⁺ ion-implanted Bakelite samples with different fluences also exhibit a similar behavior. However, the magnitude of dc conductivity is very less compared to 100 keV O⁺ ion-implanted samples. The free volume hole size of Bakelite at 150 keV O⁺ ion-implanted sample

decreases as a function of O⁺ ion fluences. However, the dc conductivity is more for O⁺ ion-implanted samples with the $10^{12} \text{ ions cm}^{-2}$ fluence. This is due to the increased movement of free ions and electrons at the surface of Bakelite. The reduced dc conductivity of Bakelite polymer at $10^{14} \text{ ions cm}^{-2}$ O⁺ ion fluence is correlated to the reduced conducting pathways by the crosslinking of polymeric chains. When the O⁺ ion fluence is $10^{15} \text{ ions cm}^{-2}$, both free volume and conductivity shows a slight increase due to the increased free volume hole size and increased mobility of the charge carries.

AC Conductivity Results

The dependency of ac conductivity upon O⁺ ion implantation at 100 keV and 150 keV at different O⁺ ion fluences are shown in Figure 8(a,b), respectively. It was observed that at all the fluences, the ac conductivity increases continuously from 100 Hz to 5 MHz. This may be due to the cleavage of polymeric chains, which will create energetic free electrons, ions and free radicals.^{24,39} The resultant conductivity is due to overall mobility of implanted ions or charge carriers in the amorphous polymer matrix, which is associated with the free volume holes.^{40,41}

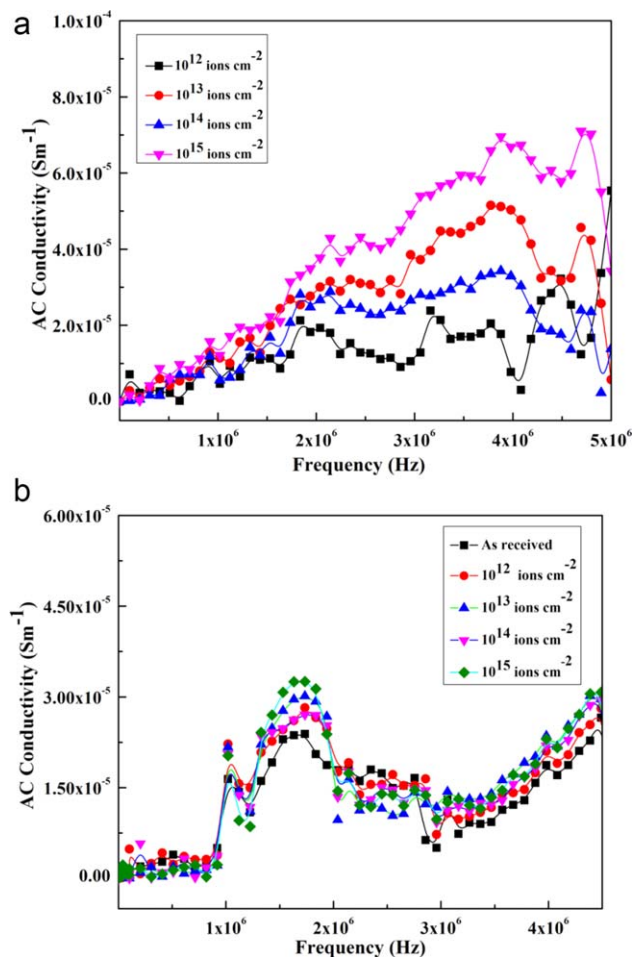


Figure 8. (a) The frequency dependence of ac conductivity of 100 keV ion-implanted Bakelite samples at different fluences. (b) The frequency dependence of ac conductivity of as received and 150 keV ion-implanted Bakelite samples at different fluences. [Color figure can be viewed at wileyonlinelibrary.com]

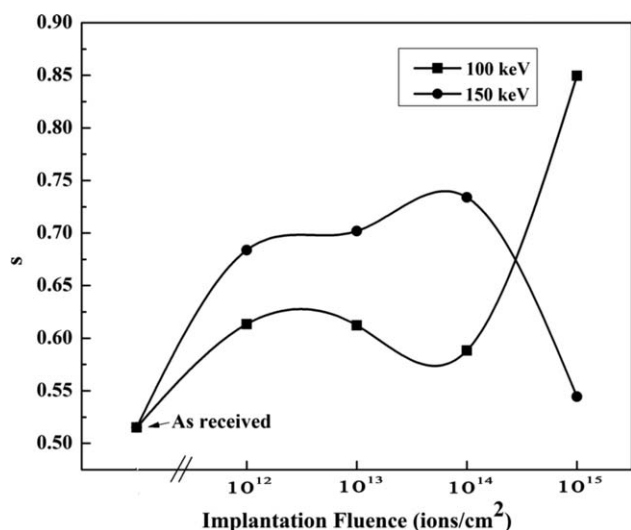


Figure 9. The variation of S value as a function of implantation fluences.

The increased free volume hole size in the polymer matrix provides pathways for the larger motion of free charge carriers/ions and facilitates the free motion of the electric dipoles. This will allow the charge carriers/ions to hop easily from conducting regions to neighbors.⁴² The conductivity of O^+ ion-implanted samples with 10^{13} to 10^{15} ions cm^{-2} fluences are more compared to the as received sample and exhibit increased free volume hole sizes. Upon implantation of 150 keV ions, the ac conductivity exhibits slightly different trend with increase in frequency of the applied field. The magnitude of the ac conductivity values are less compared to the conductivity of 100 keV O^+ ion-implanted samples due to the crosslinking of polymeric chains. From Figure 8(b), it is observed that the conductivity increases irregularly after 1.4 MHz and shows a peak at around 1.8 MHz may be due to the molecular polarization of the material medium.

A wide variety of theoretical approaches have been used to explain the behavior of ac conductivity in insulating polymers. In ac conductivity experiments, the electrical conductivity was measured as a function of frequency ω , where $\omega = 2\pi f$ is the angular frequency and " f " is the linear frequency of an alternating electric field. The empirical relation between frequency and ac conductivity $\sigma_{ac}(\omega)$ has been observed in many amorphous materials and insulators, both inorganic and polymeric materials, which is given by $\sigma_{ac}(\omega) \propto \omega^S$. This relation can be expressed as $\sigma_{ac}(\omega) = A\omega^S$, where A is a constant and S is the frequency exponent. The frequency exponent " S " is crucial in explaining the microscopic origin of the conductivity relaxation mechanism in disordered polymeric materials after ion implantation.

The variation of ac conductivity with frequency obeys Jonscher power law⁴³ especially at 100 keV ion implantation energy. A small variation observed at 150 keV is may be due to the polarization effect as mentioned by Meghna *et al.*⁴⁴ Generally, at high frequency and low temperature, the frequency exponent " S " lies between $0.5 < S < 1$.⁴⁵ The frequency exponent " S " was evaluated from the graph of $\ln \sigma_{ac}(\omega)$ versus $\ln \omega$ for the as received and ion-implanted samples. The calculated values of " S " lies

between 0.52 and 0.85 for the as received and ion-implanted samples which exhibit good agreement with the theoretically reported values.⁴⁶ The calculated values of " S " are plotted as a function of O^+ ion implantation fluences and shown in Figure 9. It is clear from the figure that " S " values at both the energies show opposite behavior with o -Ps lifetime (τ_3) and free volume size (V_f), and exhibit good agreement with the reported results in the literature.^{47,48}

CONCLUSIONS

The effects of O^+ ion implantation on the microstructure and electrical properties of polymer based Bakelite RPC detector material have been investigated. The stopping of incoming ions in the Bakelite polymer is predominantly accompanied by the deposition of high energy interior track leads to the formation of radicals, secondary ions, and electrons. Positron lifetime parameters viz., o -Ps lifetime (τ_3) and its intensity (I_3) indicate chain scission at lower fluences upon 100 keV and crosslinking at 150 keV O^+ ion implantation. Surface morphological changes upon O^+ ion implantation extremely affect the surface resistivity of the Bakelite RPC detector and their performance, which is well supported by the measured values of electrical conductivity. The increased cross linking at 150 keV at lower fluence may possibly strengthen Bakelite material due to the increased bonding of O-H pairs in the polymer structure. This will reduce the ion mobility and increase the rigidity of Bakelite structure. This is evident from the measured values of crystallinity by the XRD results. Based on these experimental results, we propose that O^+ ion implantation with the appropriate energy and fluences may reduce the leakage current and thereby enhances the detector performances in Bakelite based RPC detector material. Furthermore, optimization of oxygen ion implantation energy and fluences is essential for the improvement of Bakelite RPC detector performances and the studies on these lines are in progress.

ACKNOWLEDGMENTS

The authors are grateful to Department of Science and Technology, Govt. of India for sanctioning INO-DST Project to University of Mysore, Mysuru, vide sanction No: SR/S9/Z-01/2010 MU. We are also indebted to Inter University Accelerator Centre (IUAC), New Delhi, India, for providing the ion beam facility.

REFERENCES

- Mondal, N. K. *Pramana J. Phys.* **2012**, *79*, 1003.
- Santonico, R. *Nucl. Inst. Meth. Phys. Res. A* **2004**, *533*, 1.
- Abrescia, M.; Colaleo, A.; Iaselli, G.; Loddo, F.; Maggi, M.; Marangelli, B.; Natali, S.; Nuzzo, S. *Nucl. Inst. Meth. Phys. Res. A* **2003**, *515*, 342.
- Carlson, P.; Crotty, I.; Cwetanski, P.; Francke, T.; Fonte, P.; Peskov, V.; Sharma, A. In 48th IEEE 2001; Nuclear Science Symposium, Medical imaging Conference, San Diego, CA, **2001**; p 1.
- Arnaldi, R.; Baldit, A.; Barret, V.; Bastid, N.; Blanchard, G.; Chiavassa, E.; Cortese, P.; Crochet, Ph.; Dellacasa, G.; De Marco, N.; Drancourt, C.; Dupieux, P.; Espagnon, B.

- Ferretti, A.; Forestier, B.; Gallio, M.; Genoux-Lubain, A.; Insa, C.; Jouve, F.; Lamoine, L.; Lefevre, F.; Manso, F.; Mereu, P.; Musso, A.; Oppedisano, C.; Piccotti, A.; Poggio, F.; Royer, L.; Rosnet, Ph.; Saturnini, P.; Scalas, E.; Scomparin, E.; Sigaud, F.; Travaglia, G.; Vercellin, E. *Nucl. Inst. Meth. Phys. Res. A* **2003**, *508*, 106.
6. Goyal, P. K.; Kumar, V.; Gupta, R.; Mahendia, S.; Sharma, T.; Kumar, S. *Adv. Appl. Sci. Res.* **2011**, *2*, 227.
7. Daniel, S. G.; Kateryna, B.; Rainer, S.; Stephen, A. H.; Mohan, V. J. *Nucl. Inst. Meth. Phys. Res. B* **2015**, *360*, 54.
8. Popok, V. N. *Rev. Adv. Mater. Sci.* **2012**, *30*, 1.
9. Kavetskiy, T.; Tsmots, V.; Kinomura, A.; Kobayashi, Y.; Suzuki, R.; Mohamed, H. F. M.; Sausa, O.; Nuzhdin, V.; Valeev, V.; Stepanov, A. L. *J. Phys. Chem. B* **2014**, *118*, 4194.
10. Shariff, G.; Sathyanarayana, P. M.; Thimmegowda, M. C.; Ashalatha, M. B.; Ramani, R.; Avasthi, D. K.; Ranganathaiah, C. *Polymer* **2002**, *43*, 2819.
11. Aneesh Kumar, K. V.; Ravikumar, H. B.; Ganesh, S.; Ranganathaiah, C. *IEEE Trans. Nucl. Sci* **2015**, *62*, 306.
12. Lee, E. H.; Rao, G. R.; Mansur, L. K. *Radiat. Phys. Chem.* **1999**, *55*, 293.
13. Shaojin, J.; Zhang, Z.; Fan, Y.; Weng, H.; Zhang, X.; Hang, R. *Eur. Polym. J.* **2002**, *38*, 2433.
14. Aneesh Kumar, K. V.; Ravikumar, H. B.; Ranganathaiah, C. *J. Appl. Polym. Sci.* **2013**, *130*, 793.
15. Pradhan, D. K.; Choudhary, R. N. P.; Samantaray, B. K. *Int. J. Electrochem. Sci* **2008**, *3*, 608.
16. Hadjichristov, G. B.; Gueorguiev, V. K.; Ivanov, T. E.; Marinov, Y. G.; Ivanov, V. G.; Fau, E. *J. Phys. Conf. Ser.* **2010**, *207*, 1.
17. Kirkegaard, P.; Pedersen, N. J.; Eldrup, M. Riso National Laboratory Reports; RISO-M-274; RISO: Denmark, **1989**.
18. Nakanishi, H.; Wang, S. J.; Jean, Y. C. In *Positron Annihilation in Fluids*; Sharma, Ed.; World Scientific: Singapore, **1988**; p 292.
19. Eldrup, M.; Lightbody, D. Sherwood, *Chem. Phys.* **1981**, *63*, 51.
20. Zhang, J.; Kang, J.; Hu, P.; Meng, Q. *Appl. Surf. Sci.* **2007**, *253*, 5436.
21. Ma, B.; Wang, X.; Wu, C.; Chang, J. *Regen. Biomater.* **2014**, *1*, 81.
22. Jaleh, B.; Gavary, N.; Fakhri, P.; Muensit, N.; Taheri, S. M. *Membranes* **2015**, *5*, 1.
23. Chowdhury, P.; Mukherjee, A.; Singha, B. *Indian. J. Chem.* **2011**, *50*, 802.
24. Czvikovszky, T.; Hargitai, H. *Radiat. Phys. Chem.* **1999**, *55*, 727.
25. Iskanderova, Z. A.; Kleiman, J.; Morison, W. D.; Tennyson, R. C. *Mater. Chem. Phys.* **1998**, *54*, 91.
26. Al-Qaradawi, I. Y.; Madi, N. K.; Turos, A.; Abdul-Kader, A. M. *Radiat. Phys. Chem.* **2007**, *76*, 123.
27. Ranganathaiah, C.; Shariff, G.; Avasthi, D. K. *Radiat. Measurement.* **2003**, *36*, 629.
28. Shariff, G.; Sathyanarayana, P. M.; Thimmegowda, M. C.; Ashalatha, M. B.; Ramani, R.; Ranganathaiah, C. *Polym. Degrad. Stabil.* **2002**, *76*, 265.
29. Ismayil, Ravindrachary, V.; Bhajantri, R. F.; Praveena, S. D.; Poojari, B.; Dutta, D.; Pujari, P. K. *Polym. Degrad. Stabil.* **2010**, *95*, 1083.
30. Tao, S. J. *J. Chem. Phys.* **1972**, *56*, 5499.
31. Fink, D. *Fundamentals of Ion-Irradiated Polymers*; Fink, D., Ed.; Springer: Berlin, **2004**; p 171.
32. Kobayashi, Y.; Zheng, W.; Meyer, E. F.; Mc Gervey, J. D.; Jamieson, A. M.; Simhall, R. *Macromolecules* **1989**, *2*, 2302.
33. Tian, S.; Morris, M. F.; Morris, S. J.; Obradovic, B.; Wang, G.; Tasch, A. F.; Snell, C. M. *IEEE T. Electron. Dev.* **1998**, *45*, 1226.
34. Hasan, B. A.; Hasan, A. A.; Umran, D. A. *Int. J. Appl. Innov. Eng. Manage.* **2013**, *2*, 86.
35. Yangfei, C.; Zhiqin, C.; Liu Hongbo, X. S. *Thermochim. Acta* **2008**, *476*, 39.
36. Khanmirzaei, M. H.; Ramesh, S. *Int. J. Electrochem. Sci.* **2013**, *8*, 9977.
37. Va'vra, J. In *Nuclear Symposium Conference Record 2003 IEEE*; SLAC: Stanford, **2003**; Vol. 5, p 3704.
38. Noor, S. A. M.; Ahmad, A.; Rahman, M. Y. B. A.; Talib, I. A. *Nat. Sci.* **2010**, *2*, 190.
39. Liu, H.; Hu, X. B.; Wang, J. Y.; Boughton, R. I. *Macromolecules* **2002**, *35*, 9414.
40. Fares, S. *Nat. Sci.* **2011**, *3*, 1034.
41. Han, Z. J.; Tay, B. K.; Ha, P. C. T.; Shak-erzadeh, M.; Cimmino, A. A.; Prawar, S.; Mckenzie, D. *Appl. Phys. Lett.* **2007**, *91*, 052103.
42. Veena, M. G.; Renukappa, N. M.; Meghala, D.; Ranganathaiah, C.; Rajan, J. S. *IEEE Trans. Dielectrics Electric. Insulation* **2014**, *21*, 1166.
43. Jonscher, A. K. *Nature* **1977**, *267*, 673.
44. Meghna, K. K.; Banerjee, A.; Biswas, S.; Bhattacharya, S.; Bose, S.; Chattopadhyay, S.; Das, G.; Marick, C.; Saha, S.; Viyogi, Y. P. *IOP JINST* **2012**, *7*, 10003.
45. Hameed, M.; Ahmed; Shuja-Aldeen, B. A. *Iraqi J. Sci.* **2009**, *50*, 349.
46. El-Mallah, H. M. *Acta Phys. Polym. A* **2012**, *122*, 174.
47. El-Gamal, S.; Ismail, A. M.; El-Mallawany, R. *J. Mater. Sci. Mater. Electron.* **2015**, DOI: 10.1007/s10854-015-3391-7.
48. Ahmad, Z.; Isa, M. I. N. *Int. J. Latest Res. Sci. Technol.* **2012**, *1*, 70.